Frozen wave induced by high frequency horizontal vibrations on a CO_2 liquid-gas interface near the critical point

R. Wunenburger,[1] P. Evesque,[2] C. Chabot,[1] Y. Garrabos,[1] S. Fauve,[3] and D. Beysens[4]
[1]*Institut de Chimie de la Matière Condensée de Bordeaux, UPR 9048 du Centre National de la Recherche Scientifique, Avenue Dr. A. Schweitzer, 33608 Pessac Cedex, France*
[2]*Laboratoire de Mécanique des Sols Structures Matériaux, URA CNRS D08500, Ecole Centrale de Paris, Grande Voie des Vignes, 92295 Châtenay Malabry Cedex, France*
[3]*Laboratoire de Physique Statistique, Ecole Normale Supérieure, 24, rue Lhomond, 75231 Paris Cedex 05, France*
[4]*Département de Recherche Fondamentale sur la Matière Condensée, Commissariat à l'Energie Atomique, 17 rue des Martyrs, 38504 Grenoble Cedex 09, France*
(Received 26 October 1998)

We used the liquid-vapor equilibrium of CO_2 near its critical point ($T_C - T = 1$ to 150 mK) in order to study the stability of an interface between a gas and a liquid having close densities $\rho_L \simeq \rho_V$ when submitted to high frequency f (3–57.5 Hz) horizontal vibrations (of amplitude a from 0.1 to 2.5 mm). Above a given velocity threshold $(2\pi af)_0$ we observed a ''frozen wave,'' corresponding to an interface profile of sinelike shape which is stationary in the reference frame of the vibrated sample cell. By varying the vibration parameters, the surface tension, and the density difference between the two phases via the temperature, it was found that the wavelength and the amplitude of the stationary profile are both increasing functions of the frequency and of the amplitude of the vibration and that they are proportional to the capillary length. Our measurements are consistent with a model of inviscid and incompressible flow averaging the effect of the vibration over a period and leading to a Kelvin-Helmholtz-like instability mechanism due to the relative motion of the two fluids. [S1063-651X(99)00805-3]

PACS number(s): 47.20.−k, 64.60.−i, 64.70.Fx

I. INTRODUCTION

Vibrations applied to mechanical systems can induce destabilization or stabilization, depending on the characteristic features of the vibrations (frequency, amplitude, direction). The common effect of vertical vibrations is to modulate the effective gravity by means of the time-dependent acceleration applied to the system. For example, one of the most studied destabilizing effects of vertical vibrations is the parametric amplification of the oscillations of a system. When the hanging mass of a simple pendulum (of natural frequency f_0) is submitted to a strong vertical (i.e., parallel to Earth's gravity) vibration of frequency $2f_0$, oscillations of the pendulum at frequency f_0 are amplified. In the same way, when a strong vertical vibration of fixed frequency is applied to a vessel containing a liquid layer, one can observe oscillations of the free surface at one-half the frequency of the excitation [1] (Faraday instability). Inversely, applying high frequency vibrations can lead to the stabilization of unstable equilibrium states of the system. When the hanging mass of a pendulum is submitted to a vertical vibration of frequency f much larger than its natural frequency f_0, the unstable equilibrium position of the pendulum upside down is stabilized when $(a/l)(f/f_0) \geqslant .2\pi\sqrt{2}$ (where a is the vibration amplitude and l is the pendulum length) [2]. The corresponding hydrodynamical phenomenon is the stabilization of the free surface under a liquid layer by means of a strong vertical vibration, leading to the suppression of the Rayleigh-Taylor instability [3].

Horizontal (i.e., perpendicular to Earth's gravity) vibrations can also have nontrivial effects on the stability of mechanical systems. When the hanging mass of the pendulum is submitted to a horizontal vibration of frequency much larger than its natural frequency, above a given amplitude threshold the mean position of the pendulum is no longer vertical but makes an angle ϕ with the direction of gravity that verifies $\cos\phi = 2glf^2/a^2$ [2]. Correspondingly, a horizontal vibration of high frequency applied to a vessel containing two immiscible fluids leads to the destabilization of their initially flat interface and induces a stationary profile of sinelike shape, as first briefly reported by Wolf [3]. A theoretical explanation has been proposed by Lyubimov and Cherepanov [4]. More recently, Gonzalez-Vinas and Salan performed similar experiments [5] without reference to these previous works.

In the present work we measured the variations of the wavelength λ and amplitude A of the stationary profile observed at the interface submitted to a horizontal vibration (see Fig. 1 and comments [6]) as a function of the amplitude and frequency of the vibration. We used a two-phase system composed of a CO_2 gas-liquid equilibrium near its critical

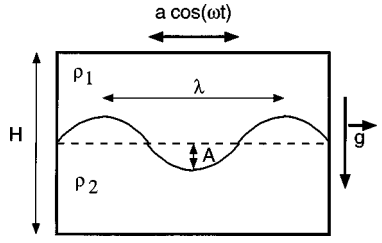

FIG. 1. Geometry of the model. Note that the thicknesses of the two fluid layers are considered as equal to $H/2$ in the model while they depend on the volume fraction x in the cells and on their orientation with respect to gravity (see Fig. 2) [6].

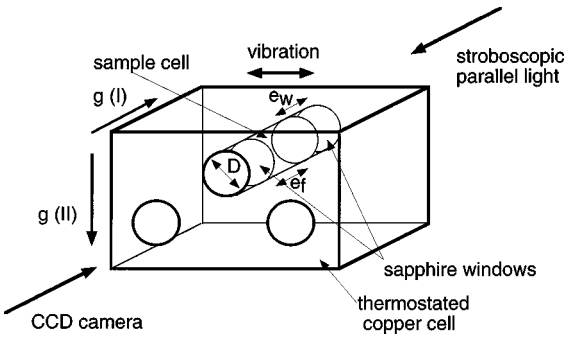

FIG. 2. Experimental setup. The top views of the interfaces are obtained when the gravity is parallel to the axis of the cells [case (I)]; the profile views of the interfaces are obtained when the gravity is perpendicular to the axes of the cells [case (II)]. Only one of the three sample fluid volumes is represented.

point. It is very useful because the surface tension and the density difference between the liquid and the gas vanish at the critical point and can be continuously adjusted by tuning the temperature. This two-phase system has another advantage: in an ordinary two-phase system composed of two fluids of close densities but of ordinaryfinite surface tension, the capillary length is often larger than the vessel (so that the dynamics of the interface is driven only by the surface tension). On the contrary, when approaching the critical point of a pure fluid, the capillary length vanishes and can be adjusted to be much smaller than the vessel size.

In Sec. II of this paper we present the experimental setup. In Sec. III we present the measurements of the wavelength of the stationary profile and compare them to the measurements of Ref. [5]. In Sec. IV we compare some of our data to a model of instability presented in Ref. [4]. Finally, in Sec. V we discuss some experimental limitations.

II. EXPERIMENTAL SETUP

The experimental setup is composed of a thermostat containing a cell with three sample fluid volumes, which is vibrated by a shaker (see Fig. 2). The thermostat has a temperature accuracy of 1 mK close to the critical temperature T_c with an operating range of (T_c, T_c-150 mK.) The shaker can apply vibrations of amplitude a and frequency f among $a=0.1$, 0.3, 1, and 2.5 mm and $f=1$, 3, 10, 30, and 57.5 Hz (a and f can be varied independently). The discretization of the vibrational parameters reflects a compromise between the technical choice concerning the shaker, the needed high level of performances of the thermostat, and the total vibrated mass. It is noteworthy that the shaker produces vibrational energy in the vibration direction and with a smaller amount, approximately 10 times less, in the plane perpendicular to the vibration direction. S-VHS video recording and image digitization are used to determine the characteristics of the interface. The cylindrical fluid volumes (of diameter D equal to 10.8 mm and of thickness e_F equal to 10.8 mm) are machined in a copper alloy cell and closed by two parallel sapphire windows (of thickness e_w equal to 9 mm). A photodiode continuously illuminates the interfaces by light transmission through the cell for vibration frequencies smaller than 30 Hz. For higher vibration frequencies the cell is illuminated by a stroboscope with a flash duration of 1 ms.

TABLE I. Normalized density differences and temperature differences $T_{\mathrm{coex}}-T_C$ of the three fluid samples, whose evolution of the volume ratio $x(T)$ is roughly indicated.

Position on pictures of the fluid samples	right	left	middle
$\delta\rho^*=(\langle\rho\rangle\text{-}\rho_c)/\rho_c$	0 ($\pm 10^{-3}$)	0.05	0.028
T_C-T_{coex} (mK)	0	7.1	1.3
volume ratio $x(T)$	constant=0.5	variable	variable

A stroboscopic frequency of 14 Hz (respectively 28 Hz) at a vibration frequency of 30 Hz (respectively 57.5 Hz) is chosen so that different phases of the vibration could be investigated at such accelerations. This frequency shift allows us to check whether the observed interface profiles are stationary in the reference frame of the cell.

The critical point of CO_2 is defined by the critical temperature $T_c=304.13$ K, the critical density $\rho_C=468\,\mathrm{kg\,m^{-3}}$, and the critical pressure $P_c=7.37$ MPa. The experimental study was performed near the critical point as characterized by the normalized density of each fluid sample and the normalized temperature distance:

$$0\leqslant\delta\rho^*=\frac{\langle\rho\rangle-\rho_c}{\rho_c}\leqslant 0.05, \tag{1}$$

$$4\times10^{-6}\leqslant\tau=\frac{T_c-T}{T_c}\leqslant 5.10^{-4}, \tag{2}$$

where $\langle\rho\rangle$ is the mean density of the fluid sample.

Three experimental fluid samples filled at different mean densities $\langle\rho\rangle$ were used (Table I). The coexistence temperature T_{coex} and the volume ratio $x(T)$ were experimentally determined for each sample at various temperatures. The volume ratio $x(T)$ is defined for each sample as the ratio of the gas volume to the total volume of the cell. From the measurements of $T_{\mathrm{coex}}-T$ and x we determined the normalized density $\delta\rho^*$ of each sample. For this we took into account the mass conservation law along the coexistence curve:

$$\Delta\rho^*=\frac{\delta\rho^*}{1-2x}, \tag{3}$$

where $\Delta\rho^*$ is the normalized density difference between the liquid phase and the vapor phase:

$$\Delta\rho^*=\frac{\rho_L-\rho_V}{2\rho_C}. \tag{4}$$

$\Delta\rho^*$ is calculated using the asymptotic scaling law (see below). For $T_c-T\leqslant 150$ mK, $\Delta\rho^*\leqslant 0.135$ [7].

III. EXPERIMENTAL RESULTS

A stationary profile of sinelike shape in the reference frame of the cell was observed only for the following pairs of parameters $(a,f)=(2.5\,\mathrm{mm}, 30\,\mathrm{Hz})$, (1 mm, 30 Hz), (0.3 mm, 57.5 Hz), (1 mm, 57.5 Hz), and (2.5 mm, 57.5 Hz). In Fig. 3 are shown snapshots of a typical profile [Fig. 3(a)] and a typical top view [Fig. 3(b)] of the interfaces observed in the

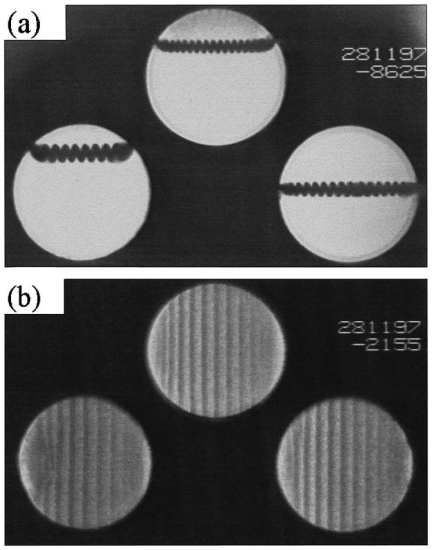

FIG. 3. Views of the three fluid samples at two different cell temperatures. (a) Profile view of the gas-liquid interfaces submitted to a vibration of frequency $f=57.5$ Hz and amplitude $a=1$ mm. The left-hand cell is at 34 mK from the critical temperature, the cell in the middle at 13 mK, the right-hand cell at 18 mK. The interface is illuminated by using a stroboscopic flash of duration 1 ms. The shape of the interface is stationary in the reference frame of the vibrated sample cell. (b) Top view of the gas-liquid interfaces submitted to a vibration of frequency $f=57.5$ Hz and amplitude $a=1$ mm. The left-hand cell is at 78 mK from the critical temperature, the cell in the middle at 57 mK, the right-hand cell at 62 mK.

three fluid samples here for a vibration at $(a,f)=(1\text{ mm}, 57.5\text{ Hz})$, at two fixed temperatures common to the cell. The variations of the wavelength λ (as defined in Fig. 1) measured at different pairs of parameters (a,f) as a function of the distance to the critical point T_c-T are displayed in Fig. 4. These variations are due to the evolution of the surface tension and of the density difference between both phases when T varies. It is noteworthy that λ is an increasing function of both f and a.

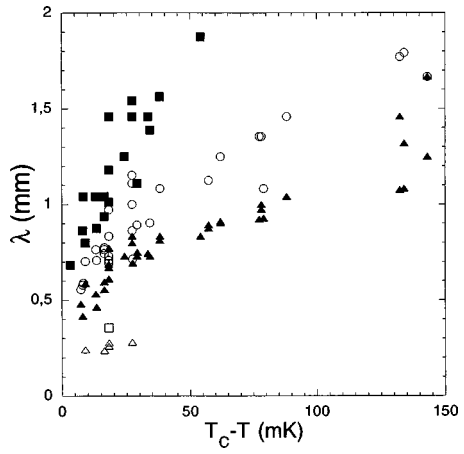

FIG. 4. Variations of the wavelength λ (mm) of the stationary profile as a function of the distance to the critical temperature T_C-T (mK) for various pairs of vibration parameters (f,a): $f=57.5$ Hz, $a=2.5$ mm (■); $f=30$ Hz, $a=2.5$ mm (○); $f=57.5$ Hz, $a=1$ mm (▲); $f=57.5$ Hz, $a=0.3$ mm (△); $f=30$ Hz, $a=1$ mm (□).

Gonzalez-Vinas and Salan [5] studied the behavior of a similar two-phase system submitted to the same kind of vibrations (frequency from 5 to 120 Hz and amplitude from 0 to 2 mm) but at larger distance from the critical point ($T_c-T=12$ K, $\Delta\rho^*=0.62$). They observed standing or propagating waves at the interface above a given value of the velocity $a\omega$. Their experimental data show that (i) the wavelength of the wave detected at the instability onset was a decreasing function of f and (ii) for $f>28$ Hz the amplitude of the vibration needed to reach the instability onset was an increasing function of f. The discretization of the frequency and of the amplitude of the vibration produced by our shaker did not allow us to detect the onset; nevertheless, we found above the onset an opposite dependence of λ with respect to f. In order to explain this discrepancy between our data and those of Ref. [5], we emphasize the fact that we observed a stationary profile at the interface in the reference frame of the sample cell, whereas the authors of Ref. [5] observed a standing or a propagating wave in the reference frame of the laboratory, i.e., a time-dependent shape. This probably indicates that we did not observe the same phenomenon here. Moreover, Gonzalez-Vinas and Salan explained the fact that λ at the onset decreases when f increases by the assumption that the walls of the vessel act as wave makers. When f is increased, wave maxima are produced at shorter time intervals, and consequently the distance between two maxima decreases due to the wave propagation. Note that this mechanism does not explain the strong dependence of λ on the vibration amplitude and that the walls can have such an effect only on propagating waves and not on a stationary profile.

IV. COMPARISON WITH A MODEL OF INSTABILITY

A. Presentation of the model

A theoretical explanation of the appearance of a stationary profile of sinelike shape at the interface has been suggested in Ref. [3] and refined in Ref. [4]. The treatment of the effects of a high frequency vibration on a mechanical system which is used in the model of Ref. [4] was first proposed by Kapitsa [2]. It describes well, for example, the effects of high frequency vibrations on a pendulum. The model of Ref. [4] is based on an instability mechanism of the Kelvin-Helmholtz type which is due to the relative motion of two fluids induced by the vibration. Under the assumption of a high vibration frequency, the fast motion (at the typical velocity $a\omega$) and the slow motion of the fluid layers (defined as their motion in the reference frame of the vibrated cell) are decoupled and it makes sense to consider only the average over one period of the effects of the vibration on the slow motion of the fluid layers. Since this average is not equal to zero because of the nonlinear dynamics of the fluid layers, it constitutes the motor of the interface instability. In order to compare our data to the predictions of the model of Ref. [4], we present it in more detail.

Two immiscible fluids of different densities (the fluid of the top layer is of density ρ_1, the fluid of the bottom layer is of density $\rho_2>\rho_1$, and for the present experiment index 1 will refer to the vapor phase whereas index 2 will refer to the

liquid phase) are supposed to be contained in a vessel of rectangular shape and of height H (H is the dimension along the gravity direction). The vessel is vibrated horizontally (Fig. 1), so that $\mathbf{x}(t)=\mathbf{a}\cos(\omega t)$, where $\mathbf{x}$ is the coordinate of any point of the cell. Fluid layers are of equal thickness. The model predicts that at a high enough frequency $f=\omega/2\pi$ and at a large enough amplitude a (these conditions will be specified later) a sinelike profile appears at the interface (''frozen wave''). This profile is stationary in the reference frame of the vessel.

The hydrodynamical modeling assumes that the flow is irrotational and incompressible. When the vibration frequency verifies $\omega \gg \nu_1/\lambda^2 \simeq \nu_2/\lambda^2$, where ν_i $(i=1,2)$ are the kinematic viscosities of the two fluids, and when the vibration amplitude verifies $a \ll \lambda$, the slow motion of the interface is decoupled from its fast motion. The onset of instability is then determined by performing a linear stability analysis. Let l_C be the capillary length:

$$1_C=\left(\frac{\sigma}{g(\rho_2-\rho_1)}\right)^{1/2}, \tag{5}$$

where σ is the interfacial tension and g is the gravity. With $\lambda_0=2\pi l_C$, a perturbation of wavelength λ becomes unstable if

$$(a\omega)^2 \geqslant \tfrac{1}{2}(a\omega)_0^2\left(\frac{\lambda}{\lambda_0}+\frac{\lambda_0}{\lambda}\right)\tanh\left(\frac{\pi H}{\lambda}\right), \tag{6}$$

where

$$(a\omega)_0^2=\frac{(\rho_2+\rho_1)^3}{\rho_1\rho_2(\rho_2-\rho_1)}\left(\frac{\sigma g}{\rho_2-\rho_1}\right)^{1/2} \tag{7}$$

is the threshold velocity which allows the instability onset to be reached. At the onset, i.e., when $a\omega=(a\omega)_0$, the wavelength of the stationary profile is equal to λ_0.

The instability condition given by Eq. (6) is very similar to the one obtained from a linear stability analysis of the classical Kelvin-Helmholtz instability. Equation (7) predicts that the threshold velocity diverges when the density ratio ρ_2/ρ_1 is large, leading to a more stable interface. According to this model, this instability should not be observed at the free surface of a container filled with water and shaken horizontally.

Since the bifurcation is supercritical, a nonlinear analysis of the instability near the onset has been performed [4]. The amplitude A of the stationary profile [under the assumption that $\lambda<H$, i.e., $\tanh(\pi H/\lambda)\simeq 1$] has the following expression:

$$A=\lambda_0\frac{2(\rho_1+\rho_2)^2}{\pi\rho_1\rho_2\left[-11\left(\frac{\rho_1}{\rho_2}\right)^2+42\left(\frac{\rho_1}{\rho_2}\right)-11\right]^{1/2}}\Delta(a\omega)^*, \tag{8}$$

where

$$\Delta(a\omega)^*=\frac{\sqrt{(a\omega)^2-(a\omega)_0^2}}{(a\omega)_0} \tag{9}$$

is the normalized distance to the velocity threshold.

Since no prediction on the evolution of λ above the onset is proposed in Ref. [4], we will (i) compare our measurements of the stationary profile amplitude to Eq. (8) and (ii) check whether our measurements of both the wavelength of the stationary profile and $\Delta(a\omega)^*$ are consistent with the prediction.

Both λ_0 and $(a\omega)_0$ depend on the thermodynamic properties of the two-phase system. Considering the small distances to the critical point at which the experiment is performed, we assume that $\Delta\rho^*$ and σ both depend on the temperature according to the asymptotic scaling laws predicted from the critical phenomena theory [7,8]:

$$\Delta\rho^* \simeq B\tau^{\beta}, \tag{10}$$

$$\sigma \simeq \sigma_0\tau^{2\nu}, \tag{11}$$

where $\beta=0.325$ and $\nu=0.63$ are the universal critical exponents; $B=1.6$ and $\sigma_0=7\ 10^{-2}\ \mathrm{N\,m^{-1}}$ are the respective values of the leading amplitudes for CO_2 [7,8].

In the vicinity of the critical point, λ_0 and $(a\omega)_0$ take the exact form

$$\lambda_0=2\pi\left(\frac{\sigma}{2g\rho_C\Delta\rho^*}\right)^{1/2}=\frac{2\pi}{\sqrt{2B}}\sqrt{\frac{\sigma_0}{g\rho_C}}\,\tau^{(2\nu-\beta)/2}, \tag{12}$$

$$(a\omega)_0=\left(\frac{2}{\Delta\rho^*}\right)^{3/4}\left(\frac{g\sigma}{\rho_C}\right)^{1/4}\frac{1}{\sqrt{1-(\Delta\rho^*)^2}}$$

$$=\left(\frac{2}{B}\right)^{3/4}\left(\frac{g\sigma_0}{\rho_C}\right)^{1/4}\frac{\tau^{(2\nu-3\beta)/4}}{\sqrt{1-B^2\tau^{2\beta}}}. \tag{13}$$

Since $\tau<4.8\times10^{-4}\ll 1$ in our experiment, $\Delta\rho^*<0.13\ll 1$, it is meaningful to develop A to the first order in $\Delta\rho^*$:

$$A=\lambda_0\left(\frac{64}{20\pi^2}\right)^{1/2}\Delta(a\omega)^*[1+\Delta\rho^*+O(\Delta\rho^{*2})]. \tag{14}$$

Asymptotically close to the critical point λ_0 scales as $\tau^{0.4675}$ whereas $(a\omega)_0$ scales as $\tau^{0.071}$. In our experimental temperature range, λ_0 remains of the order of 0.1 mm and $(a\omega)_0$ remains of the order of 100 $\mathrm{mm\,s^{-1}}$.

Let us now check if the assumptions of the model relative to the flow are verified in our experiment. First, the speed of sound vanishes at the critical point. However, its dependence on τ is weak, such that it remains approximately constant in the experimental temperature range. Its value (roughly 100 $\mathrm{m\,s^{-1}}$) is such that the corresponding acoustic wavelength is very large compared to the cell diameter D. The flow is therefore incompressible. Second, the assumption that the flow is irrotational is valid with viscous fluids if the thickness δ_i $(i=1,2)$ of the viscous boundary layers existing on each side of the interface is small compared to the interface deformation, i.e., $\delta_i \ll \lambda$ $(i=1,2)$. For a time-periodic flow of frequency f, δ_i scales as $\sqrt{\nu_i/(2f)}$. Although the viscosity differs from one phase to another and depends on the temperature, it is roughly equal in both phases and can be considered as constant in our experimental temperature range, i.e., $\nu_1\approx\nu_2\approx10^{-7}\ \mathrm{m^2\,s^{-1}}$ [9]. For $f=30$ or 57.5 Hz, δ_i $(i=1,2)$ is of the order of 0.04 mm. Considering the range of

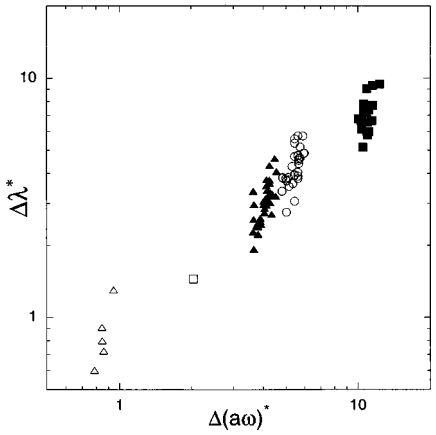

FIG. 5. Variations (in logarithmic scales) of $\Delta\lambda^*=(\lambda-\lambda_0)/\lambda_0$ as a function of $\Delta(a\omega)^*=\sqrt{(a\omega)^2-(a\omega)_0^2}/(a\omega)_0$. λ is the wavelength of the stationary profile observed at various temperatures and at various pairs of vibration parameters (f,a): $f=57.5$ Hz, $a=2.5$ mm (■); $f=30$ Hz, $a=2.5$ mm (○); $f=57.5$ Hz, $a=1$ mm (▲); $f=57.5$ Hz, $a=0.3$ mm (△); $f=30$ Hz, $a=1$ mm (□). λ_0 is the predicted wavelength at the instability onset as defined by Eq. (5), $\Delta(a\omega)^*$ is the normalized distance to the instability onset defined by Eq. (9), and $(a\omega)_0$ is the velocity threshold defined by Eq. (7).

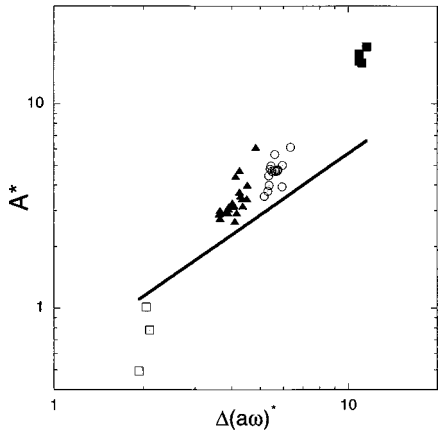

FIG. 6. Variations (in logarithmic scales) of $A^*=A/(\lambda_0(1+\Delta\rho^*))$ as a function of $\Delta(a\omega)^*$. A is the amplitude of the stationary profile observed at various temperatures and at various pairs of vibration parameters (f,a): $f=57.5$ Hz, $a=2.5$ mm (■); $f=30$ Hz, $a=2.5$ mm (○); $f=57.5$ Hz, $a=1$ mm (▲); $f=30$ Hz, $a=1$ mm (□). $\lambda_0=2\pi l_0$ is the predicted wavelength at the instability onset as defined from Eq. (5). The line corresponds to the prediction of Eq. (14). $\Delta(a\omega)^*$ is the normalized distance to the instability onset defined by Eq. (9).

wavelengths (0.25–1.5 mm) measured in this experiment, $\delta_i<\lambda$ $(i=1,2)$. Therefore, the flow can be roughly considered as a potential flow, but deviations to the predictions can be expected, particularly at short wavelengths. It is also noteworthy that the conditions of decoupling of the slow and the fast motion are only partially verified. Indeed, although the vibration frequency is large enough $(\delta_i<\lambda,\ i=1,2)$, the vibration amplitude remains large, i.e., of the same order of magnitude as the interface wavelength $(a\approx\lambda)$. The instability can occur then outside of the domain of existence predicted in Ref. [4], but again some discrepancies between the experimental data and the theory are to be expected. Moreover, due to the temperature range scanned during the experiment and to the small height of the sample cells, no density stratification occurred, so one can consider each phase as homogeneous in density (noticeable stratification is currently observed for $T_C-T\approx 1$ mK). Finally, we checked that in each geometry of the experiment the simplification $\tanh(\pi H/\lambda)\simeq 1$ is valid [6]. In conclusion, most of the assumptions of the model are verified in our experiment.

Note that the density ratio $\rho_2/\rho_1=4.09$ in the experiment reported in Ref. [5], whereas $\rho_L/\rho_V\leqslant 1.31$ in our experiment. Equation (8) predicts that the stationary profile cannot appear if $\rho_2/\rho_1>3.53$. If the model of Ref. [4] is relevant, the interface instability should not have been observed by the authors of Ref. [5].

B. Wavelength measurements analysis

In order to take the variations of the surface tension and of the density into account, we normalize the wavelength of the stationary profile to the capillary length. The variation of the reduced wavelength $\Delta\lambda^*=(\lambda-\lambda_0)/\lambda_0$ of the stationary profile as a function of the normalized distance to the velocity threshold $\Delta(a\omega)^*$ is displayed in Fig. 5. Measurements were performed at various vibration parameters (a,f) and at various temperatures. This representation of the wavelength measurements allows all the experimental data to be put on a single master curve within the experimental uncertainty. Note that $\Delta\lambda^*$ seems to be proportional to $\Delta(a\omega)^*$. At the present time we have no explanation for this linear dependence. Following the model presented above, and according to the instability condition given by Eq. (6), when $a\omega>(a\omega)_0$ many discrete wavelengths are destabilized and interact nonlinearly. Below the onsets of secondary instabilities, the resulting wavelength of the stationary profile can be very different from the most unstable wavelength at the onset.

C. Amplitude measurements analysis

From Eq. (14) we defined the normalized amplitude as $A^*=A/(\lambda_0(1+\Delta\rho^*))$ so that A^* depends only on $\Delta(a\omega)^*$ up to the second order in $\Delta\rho^*$. The variation of A^* as a function of $\Delta(a\omega)^*$ is displayed in Fig. 6. Measurements were performed at various temperatures and at various pairs of the vibration parameters (a,f). The solid line is the predicted amplitude A^* of the stationary profile obtained from Eq. (14). Note that the discrepancy between the measured and the predicted values of A^* increases with $\Delta(a\omega)^*$. This is presumably due to the fact that the use of Eq. (14) is valid only close to the onset, whereas many measurements have been performed far from the onset. It is important to note that no stationary profile has been detected for values of $a\omega$ smaller than $(a\omega)_0$. These measurements are therefore consistent with the model of a supercritical transition and with the predicted threshold, $\Delta(a\omega)^*$ being the relevant driving parameter of the instability.

V. EXPERIMENTAL LIMITATIONS

The scatter of the data has mainly three different causes. The first cause is related to the nonlinear dynamics of the

interface and to the finite size of the samples. The interface instability has been detected either by observation parallel to the interface (profiles) or by observations perpendicular to the interface (top views), depending on the orientation of the axis of the cylindrical sample with respect to gravity. In the case of measurements obtained from profiles, the finite size of the rectangular interface compared to λ leads to nonnegligible discretization of the excitable wavelengths. Concerning the wavelength measurements obtained from top views, one has to take into account not only the discretization but also the boundary effects due to the circular shape of the interface, which can modify the wavelength of the pattern and lead to the nucleation of defects. Finally, far from the onset, the nonlinear wavelength selection depends strongly on the path to attain the final vibrational conditions, and hysteresis phenomena may occur.

Another cause of the scatter of the data are the viscous effects. A strong dissipation can occur in the viscous boundary layers located along the windows when strong vibration is applied, inducing optical defocusing. The viscous dissipation occurs also along the interface, inducing local temperature gradients and local variations of the density difference and of the interfacial tension. The viscous dissipation could also slightly modify the value of the wavelength at the onset very close to T_C in an analogous way with the effect of the viscosity on the pattern at the onset of the Faraday instability [10].

Another possible cause of the scatter of the data is related to the experimental limitations due to the apparatus itself. Because of the large accelerations generated by the shaker (up to 40 g) with the camera fixed in the laboratory frame, the image resolution is somewhat speed-dependent. While in a static state the image resolution is 60 μm, it could reduce to 0.5 mm when the vessel is vibrated at $f=57.5$ Hz, $a=2.5$ mm.

In addition, we recall the current limitation of critical point experiments linked to the accuracy of the temperature regulation, which lead to a large relative uncertainty $\Delta\tau/\tau$ at small reduced temperature τ.

VI. CONCLUSION

The effect of horizontal vibrations on the stability of a fluid interface has, surprisingly, not been much studied yet, and the experimental results presented in this paper have to be considered as a first step in the comprehension of this kind of instability. The model of instability of Ref. [4] is in fair agreement with our data. Further measurements at and above the instability onset would allow the complete dependence of the wavelength of the stationary profile to be determined with respect to the characteristic features of the vibration. They would also help the role of the density difference in the dynamical coupling of both phases to be clarified. The use of a near-critical two-phase fluid where the capillary length vanishes at the critical point would help the influence of the viscosity on mechanical instabilities to be understood, as performed for the Faraday instability in Ref. [10].

ACKNOWLEDGMENTS

The authors thank G. Frohberg, J. Hegseth, B. Roux, D. V. Lyubimov, and T. Lyubimova for useful discussions, and S. Matar for his critical reading of the manuscript. This work has been supported by the European Space Agency and the CNES. A special acknowledgment is made for the technical support of DASA (Bremen, Germany), Ferrari (Modena, Italy), and Techno System (Naples, Italy).

[1] M. Faraday, Philos. Trans. R. Soc. London **52**, 299 (1831).

[2] L. D. Landau and E. M. Lifschitz, *Mécanique* (Mir, Moscow, 1973).

[3] G. H. Wolf, Z. Phys. **227**, 291 (1969); Phys. Rev. Lett. **24**, 444 (1970).

[4] D. V. Lyubimov and A. Cherepanov, Izv. Akad. Nauk SSSR, Mekh. Zhidk. Gaza **6**, 8 (1986), translated in Fluid Dyn. (USSR) **86**, 849 (1987).

[5] W. Gonzalez-Vinas and J. Salan, Europhys. Lett. **26**, 665 (1994).

[6] The cylindrical geometry of the sample cells is different from the two-dimensional rectangular cell of the model of Ref. [4] (see Fig. 1). When the axes of the cells are parallel to gravity (case I in Fig. 2), all the interfaces have a circular shape of diameter D [see Fig. 3(b)] and the thickness of each fluid layer depends on the volume fraction x. Practically, we can assume that $\tanh(\pi H/\lambda)\approx 1$. When the axes of the cells are perpendicular to gravity (case II in Fig. 2), the interfaces have a rectangular shape whose dimension along the vibration direction depends on x (from 0 mm to D). In this case the fluid layer thickness depends on x and is not constant along the vibration direction [see Fig. 3(a)]. Practically, we can still assume that $\tanh(\pi H/\lambda)\approx 1$.

[7] R. Hocken and M. R. Moldover, Phys. Rev. Lett. **37**, 29 (1976); M. R. Moldover and J. V. Sengers, Phys. Lett. **66A**, 44 (1978).

[8] J. C. Herpin and J. Meunier, J. Phys. (Paris) **35**, 847 (1974); M. R. Moldover, Phys. Rev. A **31**, 1022 (1985).

[9] G. A. Olchowy and J. V. Sengers, Phys. Rev. Lett. **61**, 15 (1988).

[10] S. Fauve, K. Kumar, C. Laroche, D. Beysens, and Y. Garrabos, Phys. Rev. Lett. **68**, 3160 (1992).